ADVANCED HEALTHCARE MATERIALS
www.advhealthmat.de

An Optimized Decellularized Extracellular Matrix from Dental Pulp Stem Cell Sheets Promotes Axonal Regeneration by Multiple Modes in Spinal Cord Injury Rats

*Wei Qiu, Bangyi Zhou, Yifei Luo, Yuanting Chen, Zehao Chen, Keke Wu, Hongle Wu, Buling Wu, Jinshan Guo, and Fuchun Fang**

In the field of tissue engineering, the extracellular matrix (ECM) is considered an important element for promoting neural regeneration after spinal cord injury (SCI). Dental pulp stem cells (DPSCs), mesenchymal stem cells that originate from the neural crest, are easy to harvest and culture in vitro, express a variety of neurotrophic factors (NTFs) and deposit a large amount of ECM, making them a good choice for stem cell- or ECM-based treatment of SCI. In the present study, decellularized extracellular matrix (dECM) derived from DPSC sheets is used for the treatment of SCI. Optimization experiments reveal that incubating DPSC sheets with 1% Triton X-100 for 5 min is the best procedure for preparing DPSC dECM. It is found that DPSC dECM promotes nerve repair and regeneration after SCI and restores hindlimb motor function in rats. Mechanistically, DPSC dECM facilitates the migration and neural differentiation of neural stem cells, as well as M2 polarization of microglia, and inhibits the formation of glial scars. This study suggests that the use of DPSC dECM is a potential strategy for the treatment of SCI.

1. Introduction

Spinal cord injury (SCI) is a devastating and complicated disorder of the central nervous system characterized by damage to spinal cord tissue, degeneration and apoptosis of neurons, and disruption of neural circuits.[1] Primary damage caused by initial mechanical injury and secondary damage caused by additional cell death, demyelination, and axonal degeneration make SCI difficult to treat.[2,3] Many clinical trials have proven that most therapeutic strategies are beneficial for improving the quality of life of patients, but the ability of these strategies to achieve neurorestoration is very limited.[4,5]

The extracellular matrix (ECM) consists mainly of collagens, proteoglycans, fibronectin, and cytokines and is considered an important element for promoting neural regeneration in the field of tissue engineering. The ECM is a dynamic network structure that not only provides structural support for cells but also plays a vital role in cell proliferation, migration, and differentiation due to its natural and specialized biological contents.[6] Recently, decellularized extracellular matrix (dECM), which is produced by removing cellular and nuclear components of cells, tissues, or organs while retaining the essential components, biological activity, and mechanical integrity of the ECM, has attracted substantial attention. It has been reported that the transplantation of dECM derived from the spinal cord,[7] brain,[8] and peripheral nerves[7] has therapeutic effects on SCI. Moreover, dECM can be prepared from cultured cells, such as mesenchymal stem cells (MSCs), after they form sheet-like structures; cell-derived dECM is

W. Qiu, B. Zhou, Z. Chen, B. Wu, F. Fang
Department of Stomatology
Nanfang Hospital
Southern Medical University
Guangzhou 510515, P. R. China
E-mail: fangfuchun@smu.edu.cn

Y. Luo
Department of Stomatology
Guangzhou First People's Hospital
School of Medicine
South China University of Technology
Guangzhou 510180, P. R. China

Y. Chen, B. Wu
Shenzhen Stomatology Hospital (Pingshan)
Southern Medical University
Shenzhen 518118, P. R. China

K. Wu
School of Biomedical Engineering
Guangzhou Medical University
Guangzhou 511495, P. R. China

H. Wu
Department of Endodontics
Stomatological Hospital
School of Stomatology
Southern Medical University
Guangzhou 510280, P. R. China

J. Guo
Department of Histology and Embryology
School of Basic Medical Sciences
Southern Medical University
Guangzhou 510515, P. R. China

The ORCID identification number(s) for the author(s) of this article can be found under https://doi.org/10.1002/adhm.202402312

DOI: 10.1002/adhm.202402312

produced under sterile conditions, has abundant sources, and is easily produced.[9] Therefore, the transplantation of cell-derived dECM has become a potential strategy for the treatment of SCI. Several studies have demonstrated that mesenchymal cell-derived dECM can promote neural regeneration.[10–12] However, the therapeutic effect of MSC-derived dECM transplantation on SCI has not been determined.

Dental pulp stem cells (DPSCs) are MSCs that can differentiate into osteoblasts, chondrocytes, adipocytes, and neurons.[13–15] DPSCs might be more neurogenic than BMSCs (Bone marrow mesenchymal stem cell) due to their neural crest origin.[16] In addition, DPSCs are easy to harvest and culture in vitro,[17] express a variety of neurotrophic factors (NTFs)[18] and deposit a large amount of ECM,[19] making them good choices for stem cell and/or dECM-based SCI treatment. Current research has found that loading DPSCs on prevascularized scaffolds[20] or hydrogels[21] can significantly enhance their therapeutic effects on SCI in rats. Direct transplantation of DPSC overexpressing bFGF[22] can also improve the local hypoxic microenvironment at the site of SCI in rats, thereby achieving the goal of repairing SCI. Therefore, studying the effects of DPSC-derived ECM or dECM is highly important for developing strategies to promote neural repair and regeneration after SCI.

In this study, dECM derived from DPSC sheets was prepared for the treatment of SCI. We investigated the characteristics of this ECM, including its histological appearance, ultrastructure, DNA content and cytotoxic effects, to determine the optimal preparation conditions. Then, cell sheets and dECM were transplanted into rats with T10 hemisection to assess whether they could promote axonal regeneration and functional recovery. Finally, the effect of dECM in regulating the migration and differentiation of NSCs (Neural stem cells) was also investigated.

2. Results

2.1. Multidirectional Differentiation Potential of DPSCs

After nearly 14 days of culture, cells that were extracted from the dental pulp adhered to the culture dishes and exhibited a fibroblast-like morphology (**Figure 1A**). The DPSCs used in this study were obtained using a limited dilution technique (Figure 1B,C). The flow cytometry results revealed that DPSCs were positive for CD29, CD44, CD90, and CD105 and negative for CD34 and CD45 (Figure 1D). Staining with Alizarin red and Oil Red O was used to confirm the multipotency of the DPSCs after 14 days of culture under osteogenic and adipogenic conditions (Figure 1E,F). After 14 days of culture under neurogenic conditions, the DPSCs exhibited distinctive morphologies that ranged from extensively simple bipolar to large, branched multipolar cells (Figure 1G). Subsequently, the qRT–PCR results suggested that the expression of the neurogenic markers nestin, β3-TUBULIN, GAP43, and NF (Neurofilament) was upregulated (Figure 1H–K).

2.2. Characteristics of DPSC Sheets Before and After Decellularization

After 14 days of continuous culture with a high concentration of ascorbic acid, the seeded DPSCs formed an ivory white translucent sheet that could be easily mechanically detached from the dish and easily handled with forceps (**Figure 2A-a**). After being decellularized with different concentrations of Triton X-100 for different durations (0.5% Triton X-100 for 5 min, 0.5% Triton X-100 for 10 min, 0.5% Triton X-100 for 30 min, 1% Triton X-100 for 5 min, 1% Triton X-100 for 10 min and 1% Triton X-100 for 30 min), the DPSC sheets became more transparent and smaller in size (Figure 2A-b–g). Among that in the different treatment groups, the dECM in the 1% Triton X-100 30 min group decreased in size to the greatest degree. H&E staining revealed that the DPSC sheets were composed of multiple layers of cells and the ECM that they secreted (Figure 2B-a). After decellularization, the majority of the DPSCs that were previously present in the cell sheet were successfully removed, as shown in Figure 2B-b–g). However, residual nucleic acid was observed in the 0.5% Triton X-100 5 min group (Figure 2B-b yellow arrow). DNA content was 3866 ± 214.0 ng mL^{-1} in the DPSC sheet group but decreased to 173.1 ± 4.555 ng mL^{-1} in the 0.5% Triton X-100 5 min group, 95.27 ± 10.20 ng mL^{-1} in the 0.5% Triton X-100 10 min group, 76.83 ± 4.698 ng mL^{-1} in the 0.5% Triton X-100 30 min group, 49.62 ± 10.63 ng mL^{-1} in the 1% Triton X-100 5 min group, 26.50 ± 4.521 ng mL^{-1} in the 1% Triton X-100 10 min group and 7.436 ± 4.372 ng/mL in the 1% Triton X-100 30 min group (Figure 2C). More than 99% of the DNA in the DPSC sheet was removed in the 1% Triton X-100 10 min group and 30 min group, and the removal of this much DNA might have impaired the integrity of the ECM.[23] Cytotoxicity analyses with the CCK8 assay demonstrated no significant difference in absorbance among the different groups (Figure 2D), suggesting that the decellularized DPSC sheets had no cytotoxic effect on NSCs and could be used in animal studies.

2.3. Microstructural Observation and Immunofluorescence Staining of DPSC Sheets Before and After Decellularization

SEM (Scanning electronic microscopy) showed that the DPSCs were embedded in their own secreted ECM, grew in multiple layers (**Figure 3A-a**), and were closely connected to the ECM that surrounded the cells with many tiny fibrin fibers visible at high magnification (Figure 3A-a'). After cell removal by incubation with different concentrations of Triton X-100, the vast majority of the DPSCs were removed from the original cell sheet (Figure 3A-b–g). At high magnification, the collagen structures were arranged more regularly and more densely in the 0.5% Triton X-100 5 min group and 1% Triton X-100 5 min group than in the other groups (Figure 3A-b',e'). When the processing time reached 10 and 30 min, the ECM structure was severely disrupted, and collagen was sparser and more irregularly aligned than in the original DPSC sheets (Figure 3A-c',d',f',g'). Immunofluorescence staining of collagen I was used to assess the integrity of the ECM structure, and a well-developed network of collagen fibers was observed before decellularization (Figure 3B-a). After decellularization, the components of the ECM were well preserved (Figure 3B-b–g), and there was no significant difference in fluorescence intensity (Figure 3C). However, nuclei, which were stained blue, were found in the 0.5% Triton X-100 5 min group (Figure 3B-b), suggesting that the cell components were not completely

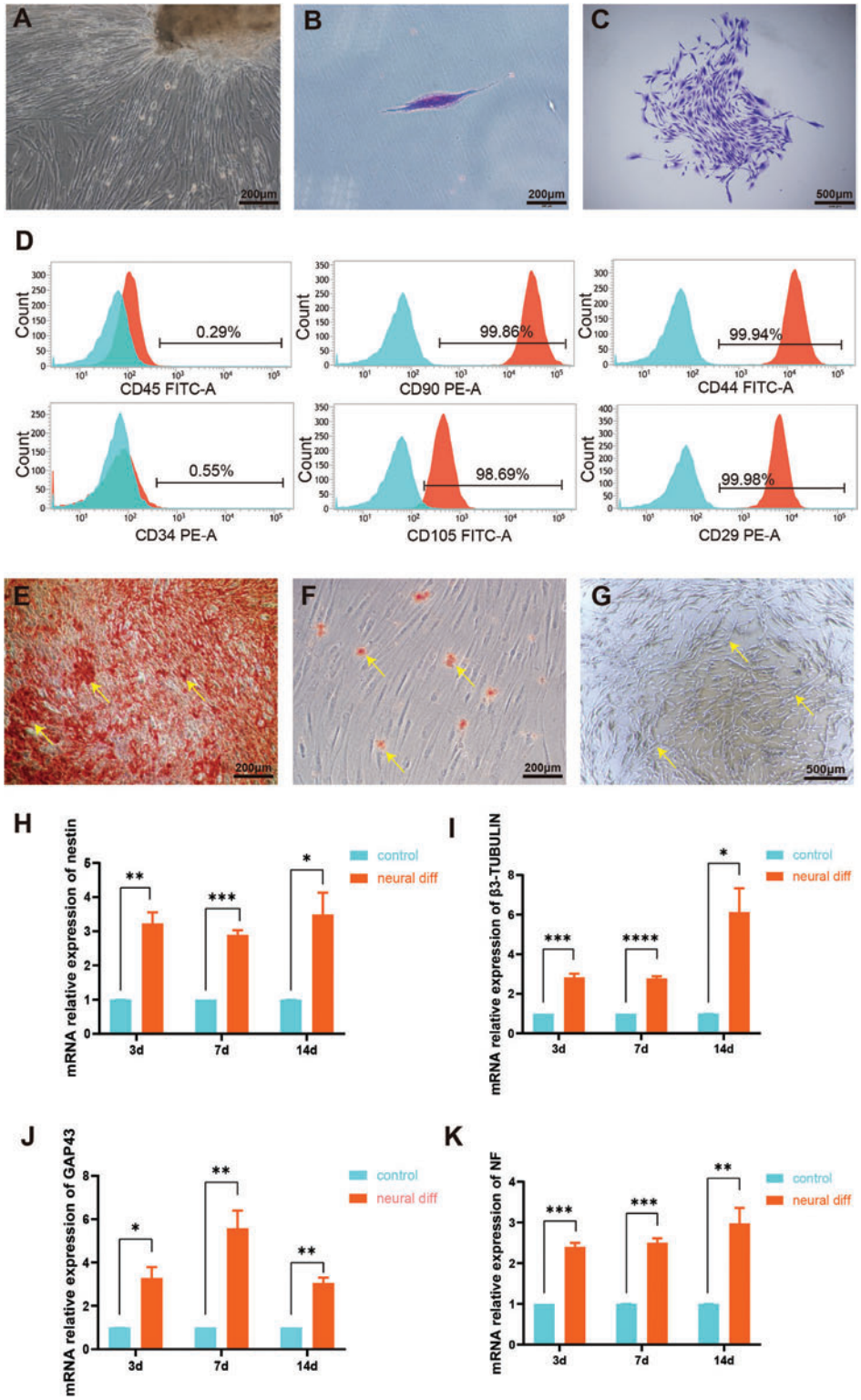

Figure 1. Identification and multi-differentiation potential of DPSCs. A) Primary cultured DPSCs. B) Single cells were obtained. C) Single cell-derived colonies were obtained after culture for 14 days. D) Flow cytometric analysis of the expression of surface markers of DPSCs. DPSCs were positive for CD29 (99.88%), CD44 (99.94%), CD90 (99.86%), and CD105 (98.69%) and negative for CD34 (0.55%) and CD45 (0.29%). E) The yellow arrows indicate mineralized nodules formed in the osteogenic differentiation group. F) The yellow arrows indicate lipid droplets formed in the adipogenic differentiation group. G) The yellow arrows indicate branched multipolar cells in the neurogenic differentiation group. H–K) The expression levels of nestin, β3-TUBULIN, GAP43, and NF increased in the neurogenic differentiation group on days 3, 7, and 14, as determined via qRT–PCR ($n = 3$). The data represent the mean ± SE. *P < 0.05, **P < 0.01, ***P < 0.001, ****P < 0.0001; two-tailed t test.

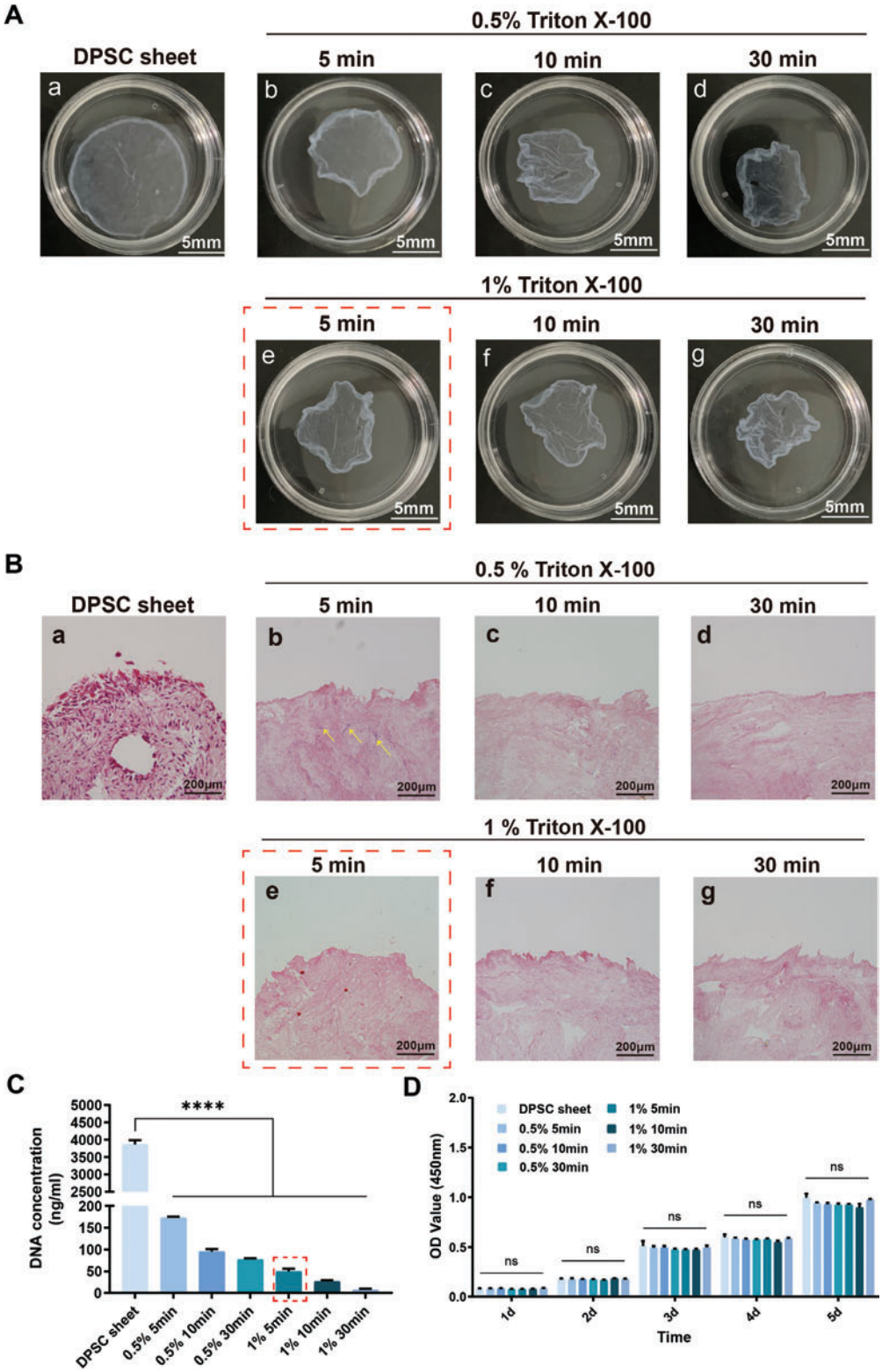

Figure 2. Characteristics of DPSC sheets before and after decellularization. A) After 14 days of culture, the seeded DPSCs formed an ivory white translucent sheet. DPSC dECM from the different groups after decellularization (0.5% for 5 min, 0.5% for 10 min, 0.5% for 30 min, 1% for 5 min, 1% for 10 min, and 1% for 30 min). B) H&E staining of DPSC sheets before and after decellularization. The yellow arrows indicate the residual nuclear contents in the 0.5% Triton X-100 5 min group. C) Quantification of DNA content in the different groups. The optimum treatment condition was 1% Triton X-100 for 5 min ($n = 3$). D) In the CCK-8 assay, there were nonsignificant differences in absorbance among the different groups ($n = 3$). The data represent the mean ± SE. ****$P < 0.0001$; one-way ANOVA followed by Tukey's multiple comparisons test.

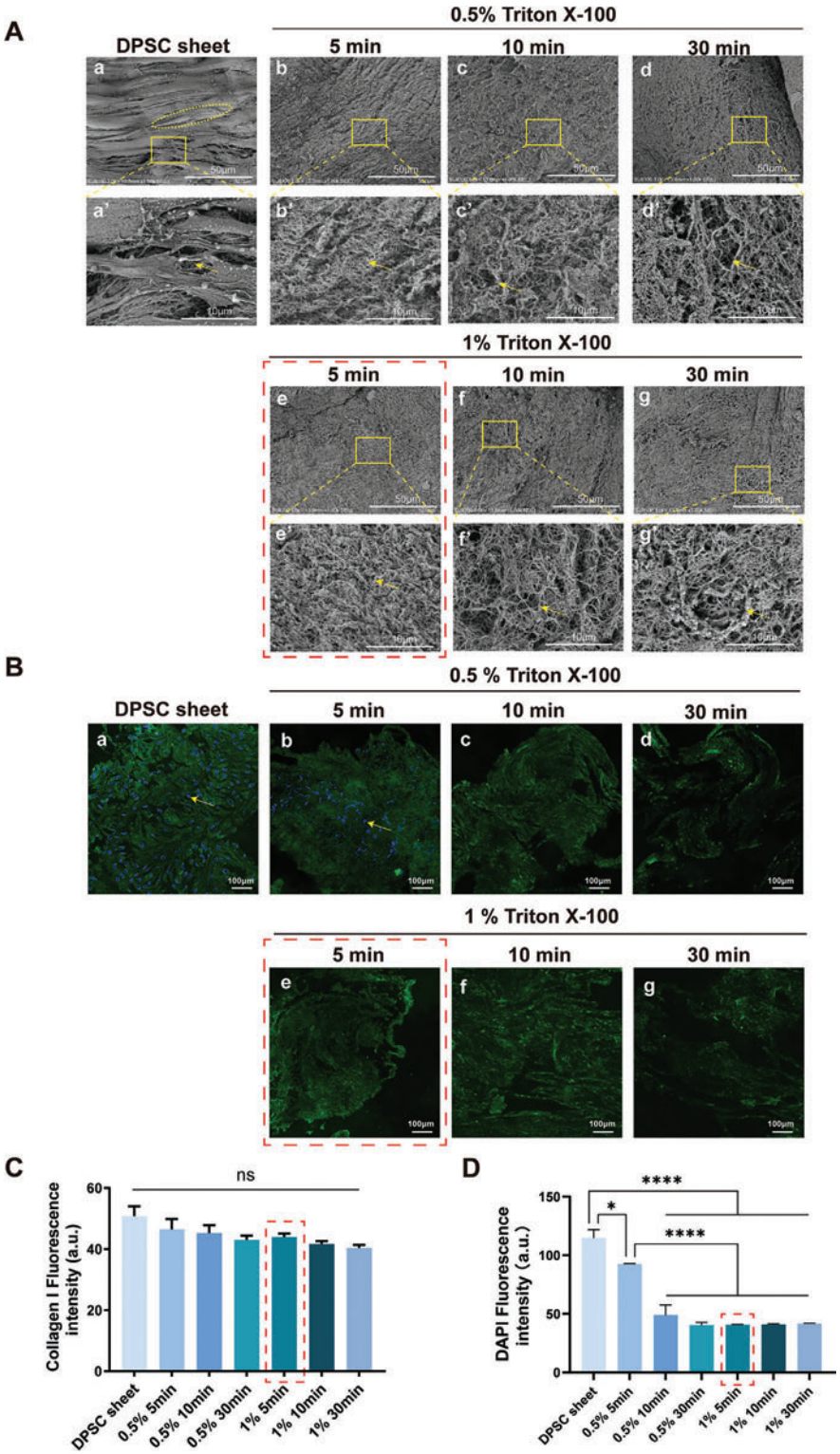

Figure 3. Microstructural observation and immunofluorescence staining of DPSC sheets before and after decellularization. A) SEM image of DPSC sheets before decellularization. DPSCs were embedded in their self-secreted endogenous ECM. The dotted circle shows a single cell. A-b–g) After decellularization, the vast majority of the DPSCs were removed from the sheets in the different groups. A-a'–g') High-magnification SEM images of DPSC sheets after decellularization. The yellow arrows indicate fibrin fibers. The optimum treatment condition was 1% Triton X-100 for 5 min. B) Immunofluorescence staining of collagen I in DPSC sheets before and after decellularization. The yellow arrows indicate nuclei, which were stained using DAPI. C,D) The fluorescence intensities of collagen I and DAPI in the different groups are shown in (B). The data represent the mean ± SE (n = 3). *P < 0.05, ****P < 0.0001; one-way ANOVA followed by Tukey's multiple comparisons test.

removed, which was consistent with the results of H&E staining (Figure 3D).

Together with the H&E staining and DAPI staining results, these data demonstrated that incubation with 1% Triton X-100 for 5 min thoroughly removed cellular components, while incubation with 0.5% Triton X-100 for 5 min did not. Moreover, immunofluorescence staining for collagen I and SEM analysis showed that the structure of the ECM in the 1% Triton X-100 5 min group was well preserved. Therefore, the optimal Triton X-100 concentration and treatment duration for decellularizing DPSC sheets were 1% Triton X-100 and 5 min. Subsequently DPSC dECM was transplanted into SCI model rats to investigate its therapeutic effect.

2.4. DPSC dECM Improved the Locomotor Function of SCI Model Rats

Figure 4A,B shows the schematic diagram of the SCI modeling procedure and experimental time course. A rat model of T10 spinal cord hemisection was successfully established, and DPSC dECM or DPSC sheets were transplanted into the lesion side (Figure 4C). After SCI, the right legs of the animals were paralyzed. The recovery of locomotor function was assessed by footprint analysis and Basso-Beattie and Bresnahan (BBB) scores. The animals were divided into three groups (the control group, DPSC sheet group, and DPSC dECM group). Over 28 days, the motor function of all the animals gradually improved (Videos S1–S3, Supporting Information), and footprint analysis showed that the control group had more severe gait dysfunction, specifically on the affected side, than the DPSC sheet group and DPSC dECM group (Figure 4D). In addition, compared with those of the control group, the BBB scores of the DPSC sheet group and DPSC dECM group were significantly improved (Figure 4E). However, there were no statistically significant differences between the DPSC sheet group and the DPSC dECM group. Collectively, these results demonstrated that compared with those in the control group, rats in the DPSC sheet group and DPSC dECM group exhibited improved locomotor functional recovery.

2.5. DPSC dECM Reduced the Area of Injury in SCI Model Rats

The spinal cords of rats in each group were collected on day 7 and day 28 after transplantation (**Figure** 5A,B). The lesion size was reduced in the DPSC sheet and DPSC dECM groups compared with the control group on day 7 and day 28. The defect areas in the control group were the largest on day 7 and day 28, specifically (70.75 ± 13.53)% and (34.10 ± 10.93)%, respectively. The defect areas of the DPSC sheet group were (18.31 ± 3.589)% on day 7 and (8.596 ± 4.891)% on day 28. The defect areas of the DPSC dECM group were (12.19 ± 1.918)% on day 7 and (4.708 ± 3.394)% on day 28, which indicated that transplantation of DPSC dECM promoted tissue repair after SCI (Figure 5C,D). However, there was no significant difference between the DPSC dECM group and the DPSC sheet group in terms of the reduction in the spinal cord lesion size.

2.6. DPSC dECM Promoted Axonal Regeneration and Reduced the Formation of Glial Scars in SCI Model Rats

To further investigate the histological changes induced by DPSC dECM treatment and the mechanism underlying the ability of DPSC dECM to promote functional recovery after SCI, the localization of NSCs was evaluated to assess local NSC recruitment and neural regeneration. Compared to that in the control group, the defect areas in the treatment groups were significantly decreased, which was similar to the results of HE staining (**Figure 6**B,E,H,K). NSCs were labeled with nestin, neurons were labeled with NF, astrocytes were labeled with GFAP (Glial fibrillary acidic protein), and the glial scar was labeled with CS56. At 3 dpi, nestin-positive cells appeared at the injury site in the DPSC sheet group and DPSC dECM group, while almost no nestin-positive cells were observed in the control group (Figure 6A,C). At 28 dpi, NF-positive neurons were located at the center of the injury site in the DPSC sheet group and DPSC dECM group, while the control group exhibited markedly lower NF expression (Figure 6D,F). The DPSC sheet group and DPSC dECM group also exhibited a significantly lower fluorescence intensity of CS56 than the control group at 28 dpi (Figure 6G,I). DPSC dECM and DPSC sheets reduced glial scar formation, induced neurite sprouting (NF+) toward the lesion gap and increased tissue repair, which led to improved locomotor function after SCI.

2.7. DPSC dECM Regulated the Immune Microenvironment

The transition of microglia/macrophage from the proinflammatory M1 phenotype to the anti-inflammatory M2 phenotype may be particularly important in promoting spinal cord tissue repair. Therefore, we conducted CD68 immunofluorescence staining to elucidate the phenotypes of macrophages/microglia. Additionally, we performed colabeling for CD206 to precisely identify and assess the localization of M2 macrophages/microglia. The results showed that compared with the control group, there was no significant change in the number of activated macrophages in the DPSC sheet group and DPSC dECM group, but the percentage of M2 macrophages significantly increased ($P < 0.01$) (Figure 6J,L,M), indicating implantation of DPSC sheets and DPSC dECM regulated the immune microenvironment.

2.8. DPSC dECM Facilitated NSC Migration and Neural Differentiation

Figure 7A shows a schematic diagram of the NSC transwell chemotaxis assays. As shown in Figure 7B, compared with the control treatment, DPSC sheets and DPSC dECM promoted the migration of NSCs. However, there was no significant difference in the number of migrating NSCs between the DPSC sheet group and the DPSC dECM group ($P > 0.05$), indicating that there was no significant difference in the extent of NSC migration between the DPSC sheet group and the DPSC dECM group (Figure 7C); these results suggested that DPSC sheets or DPSC dECM could promote the migration of NSCs.

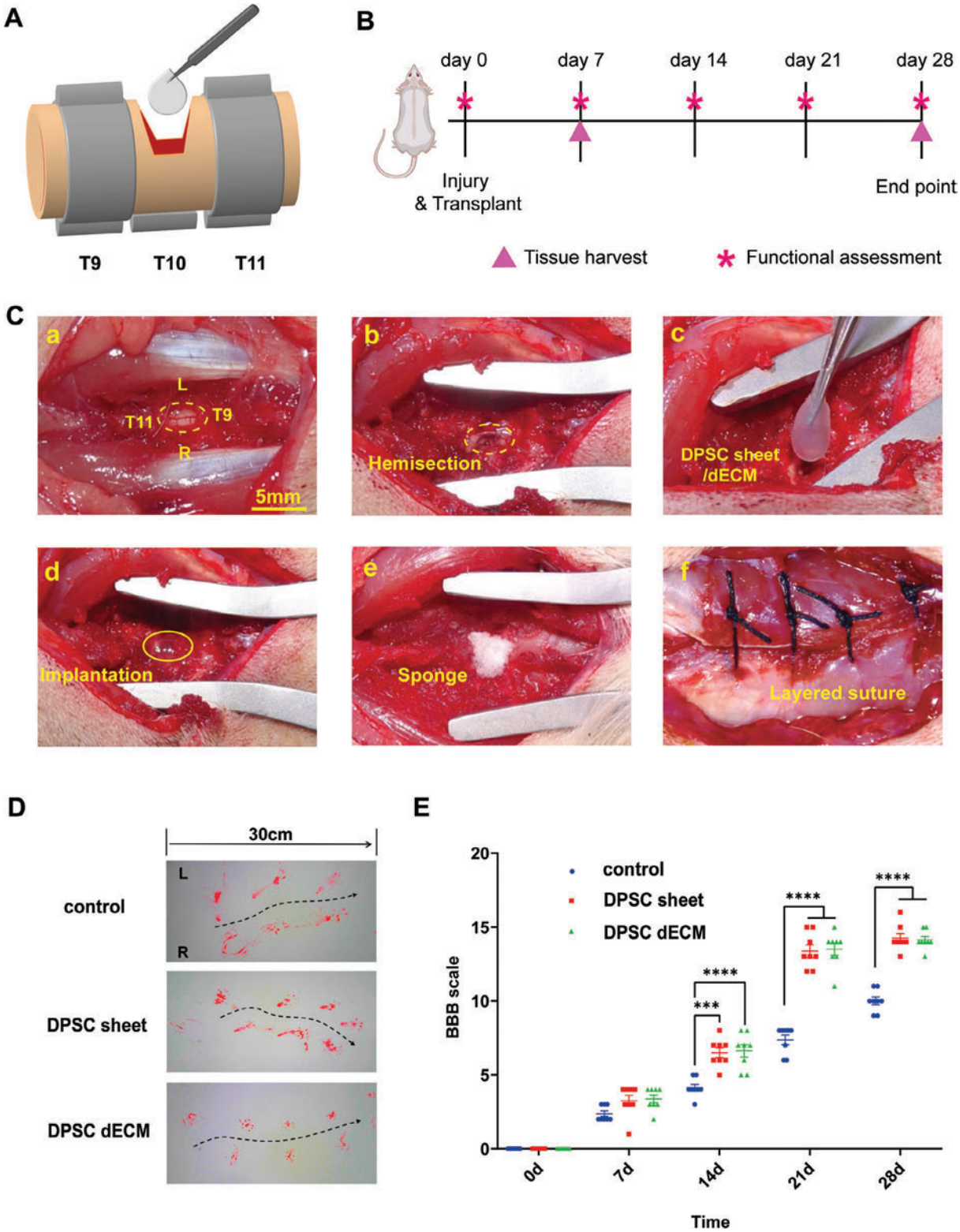

Figure 4. DPSC dECM improved locomotor function in rats with SCI. A) Schematic diagram of the T10 spinal cord hemisection model. B) Time course of DPSC dECM transplantation, behavioral assessment, and tissue harvesting. Tissue was harvested on day 7 and day 28 after transplantation. Behavioral assessments were performed weekly following transplantation. C) A rat T10 spinal cord hemisection model was successfully constructed. D) Footprint analysis of rats in the control group, DPSC sheet group, and DPSC dECM group on day 28 ($n = 3$). E) BBB scores of rats in the control group, DPSC sheet group, and DPSC dECM group ($n = 8$). The data represent the mean ± SE. ***P < 0.001, ****P < 0.0001; one-way ANOVA followed by Tukey's multiple comparisons test.

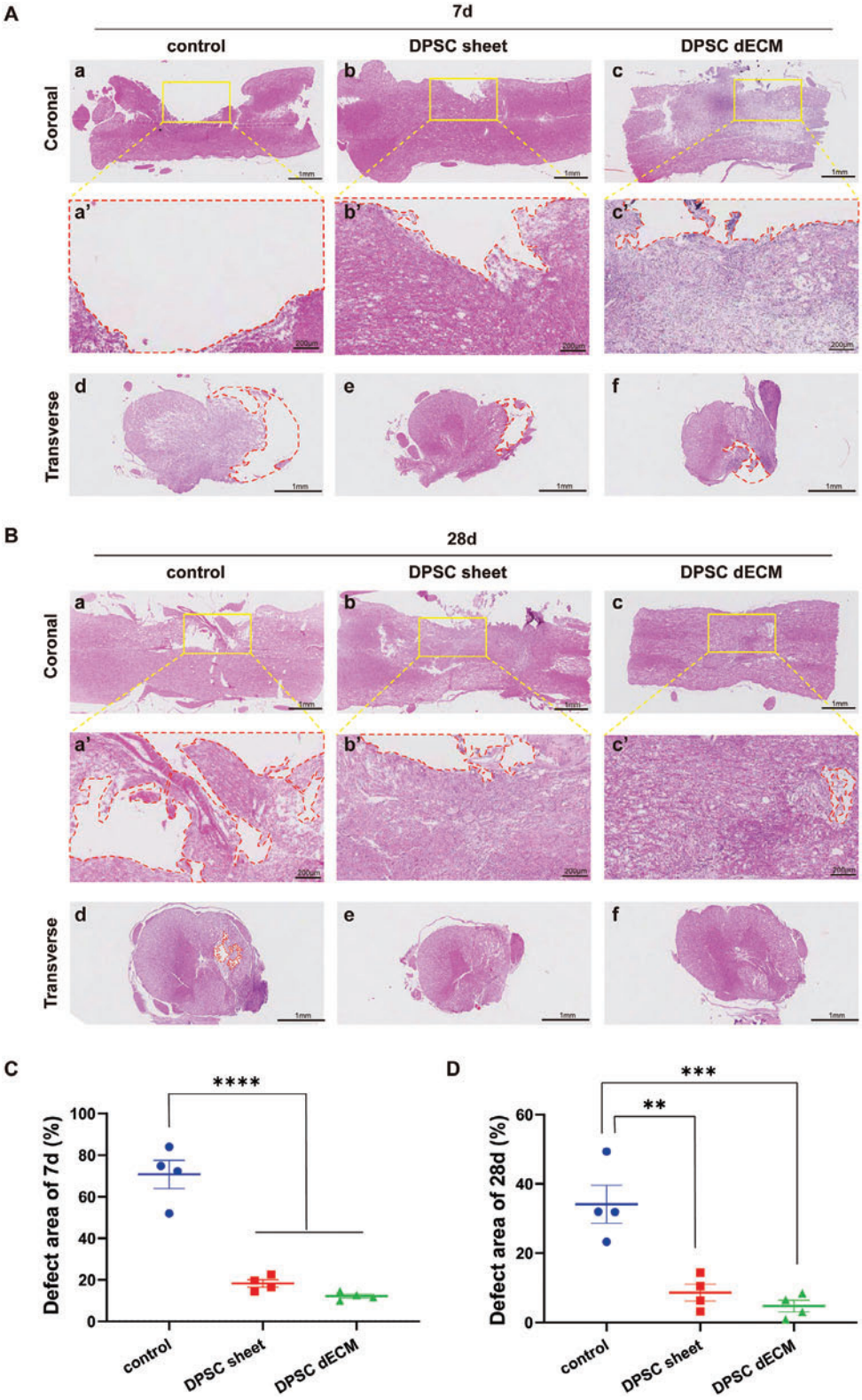

Figure 5. DPSC dECM reduced the area of injury in rats with SCI. A,B) Coronal and transverse H&E-stained sections obtained on day 7 and day 28 after SCI. The yellow boxes represent the ROIs, which had a length of 2 mm and a width of the distance from the centerline to the edge of the tissue. The red dotted line shows the defect areas in the different groups. C,D) Quantification of the defect area in the control group, DPSC sheet group and DPSC dECM group on day 7 and day 28. The data represent the mean ± SE ($n = 4$). **P < 0.01, ***P < 0.001, ****P < 0.0001; one-way ANOVA followed by Tukey's multiple comparisons test.

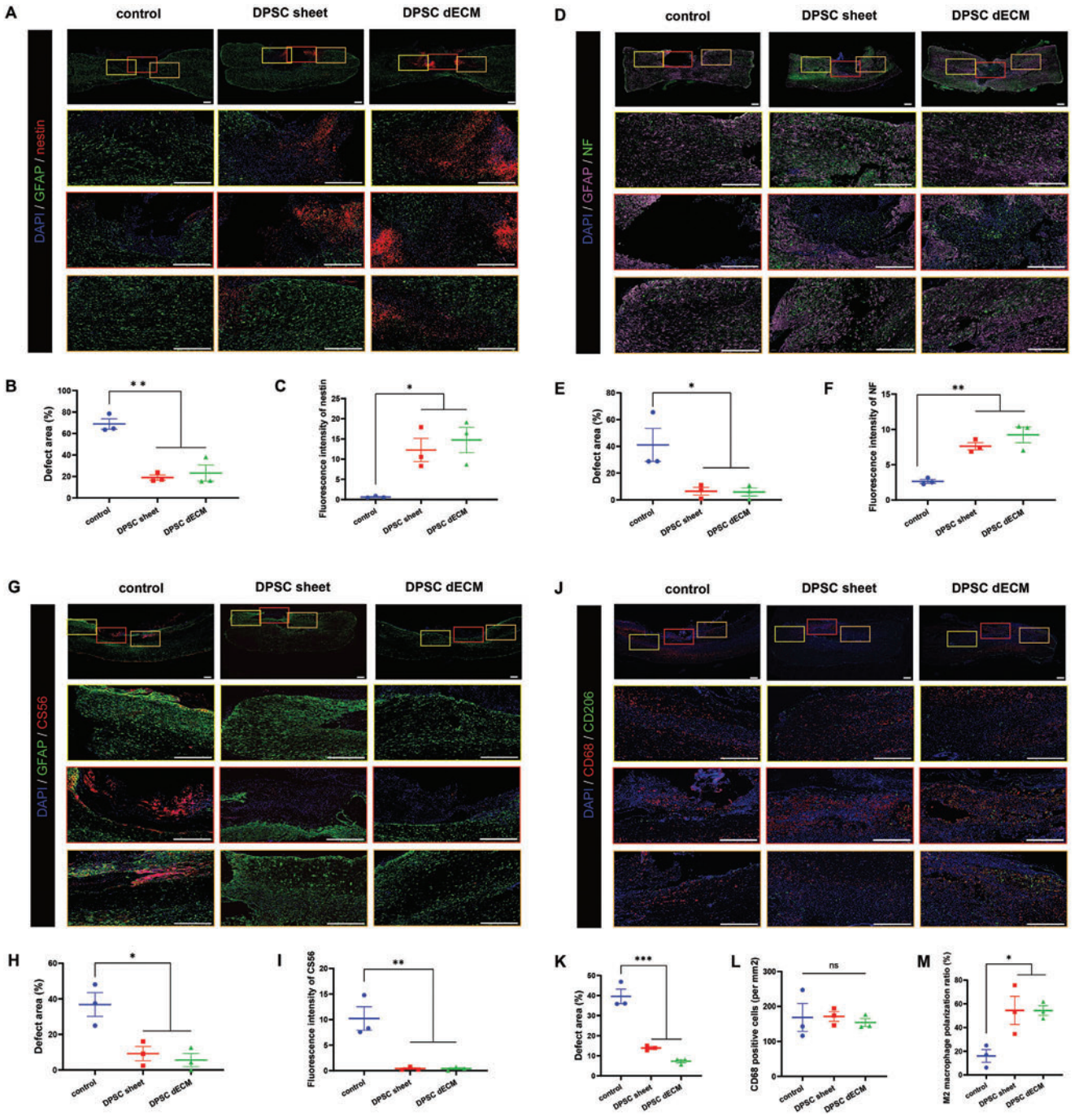

Figure 6. DPSC dECM promoted neural regeneration in rats with SCI. A) DPSC sheets and DPSC dECM promoted NSC migration 3 dpi. Green represents the astrocytic marker GFAP, and red represents the NSC marker nestin. B,C) Quantification of the defect areas and nestin IF intensities in the three groups. D) DPSC sheets and DPSC dECM promoted neural regeneration 28 dpi. Green represents the neuronal marker NF, and purple represents the astrocytic marker GFAP. E,F) Quantification of the defect areas and NF IF intensities in the three groups. G) DPSC sheets and DPSC dECM reduced the formation of glial scars 28 dpi. Green represents the astrocytic marker GFAP, and red represents the glial scar marker CS56. H,I) Quantification of the defect areas and CS56 IF intensities in the three groups J) DPSC sheets and DPSC dECM regulated the immune microenvironment. Red represents the macrophage/microglia marker CD68, and green represents the M2 macrophage/microglia marker CD206. K–M) Quantification of the defect areas, activated macrophages and percentage of M2 macrophages in the three groups. The yellow box represents the rostral, the red box represents the injury site, and the orange box represents the caudal. Scale bars: 500 μm. The data represent the mean ± SE ($n = 3$). *P < 0.05, **P < 0.01, ***P < 0.001; one-way ANOVA followed by Tukey's multiple comparisons test.

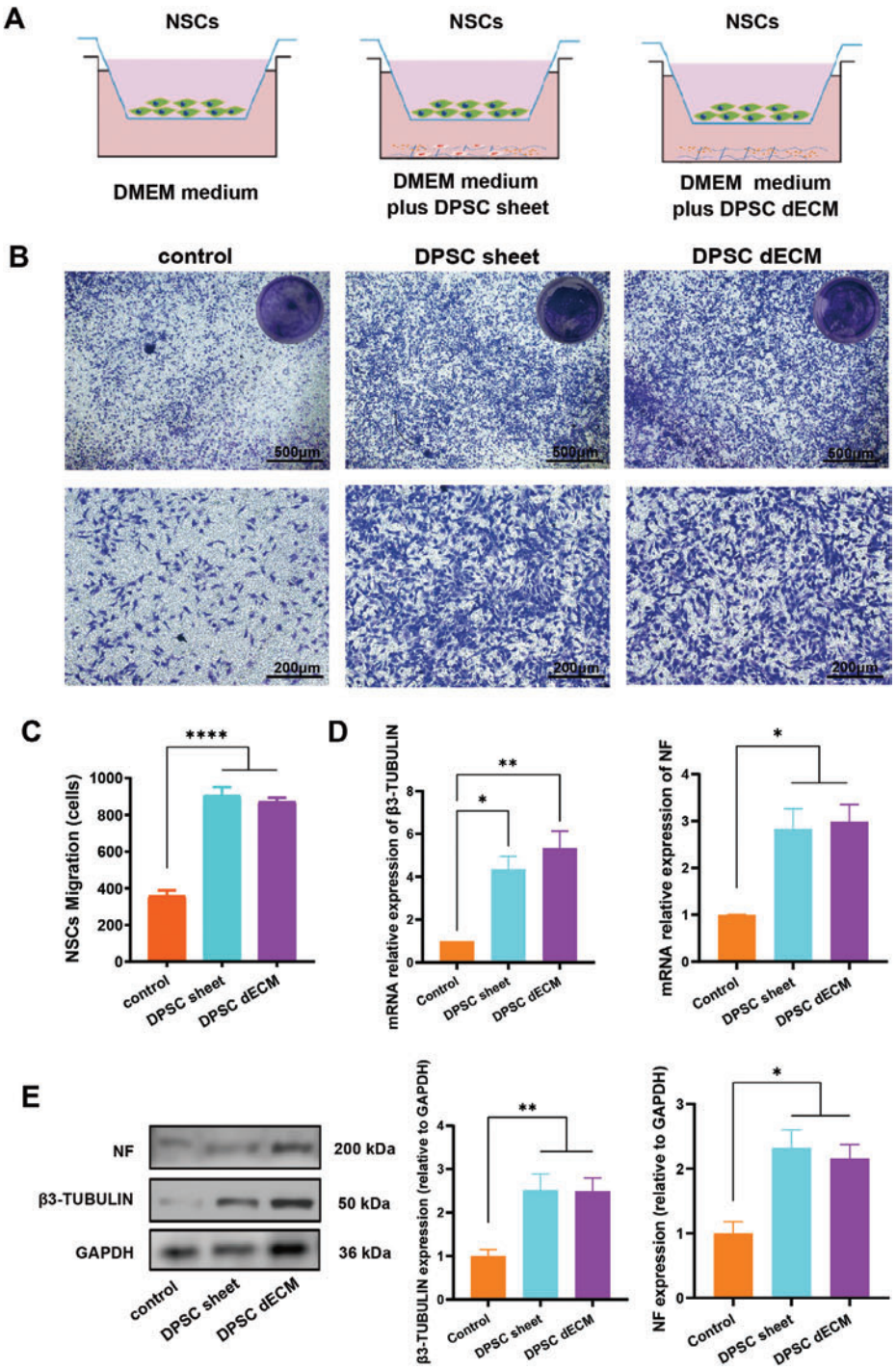

Figure 7. DPSC dECM promoted NSC migration and neural differentiation. A) Diagram of NSC chemotaxis in transwell plates mediated by DPSC sheets and DPSC dECM. B) Comparison of the effects of DPSC sheets and DPSC dECM on the migration of NSCs. C) Migrated NSCs were counted in the different groups. D) The expression levels of β3-TUBULIN and NF of NSCs increased after co-culture with DPSC sheets and DPSC dECM using qRT-PCR. E) Western blot analysis showed that β3-TUBULIN and NF protein expressions were increased after coculture with DPSC sheets and DPSC dECM. The data represent the mean ± SE ($n = 3$). *P < 0.05, **P < 0.01, ****P < 0.0001; one-way ANOVA followed by Tukey's multiple comparisons test.

Western blotting analysis and qRT-PCR revealed that the expressions of β3-TUBULIN and NF in the coculture groups, including the NSC and DPSC sheet coculture group and the NSC and DPSC dECM coculture group, were significantly higher than those in the control group (Figure 7D,E). However, the levels of β3-TUBULIN and NF were not significantly different between the DPSC sheet group and the DPSC dECM group. Collectively, these results suggest that both DPSC sheets and DPSC dECM promoted the migration and neural differentiation of NSCs.

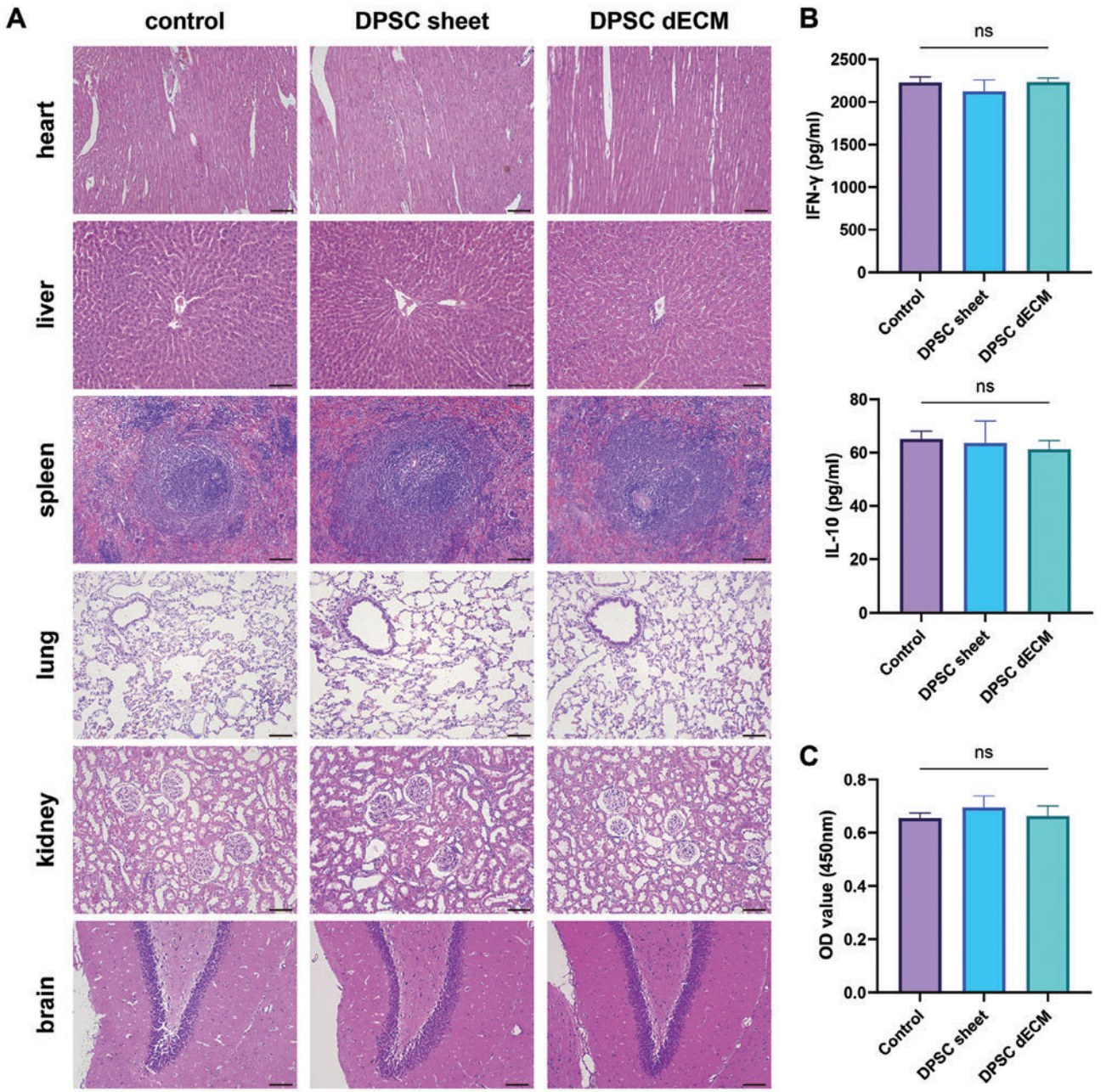

Figure 8. DPSC dECM had a favorable safety profile. A) HE staining of the heart, liver, spleen, lung, kidney, and brain 28 dpi. B) IFN-γ and IL-10 levels in the serum of the rats among three groups 28dpi measured by ELISA. C) After co-culture with C17.2 in vitro, the CCK-8 assay shows no difference among the three groups. The data represent the mean ± SE ($n = 3$). One-way ANOVA.

2.9. DPSC dECM Possessed a Favorable Safety Profile

To further explore the potential of DPSC dECM for clinical application, we assessed posttransplantation immune rejection and potential histopathological changes in several major organs of the rats. As expected, the EILSA results showed no significant difference in IFN-γ or IL-10 levels in the serum of the rats among three groups, indicating that DPSC sheet and DPSC dECM transplantation did not result in immune rejection (**Figure** 8B). Moreover, histopathological sections of the heart, liver, spleen, lung, kidney, and brain showed no abnormalities and the CCK8 assay showed no difference among the three groups after co culturing with C17.2 in vitro, indicating that the DPSC sheets and DPSC dECM had high biosafety (Figure 8A,C).

3. Discussion

The results of the present study indicate that 1% Triton X-100 for 5 min was the best condition for producing DPSC dECM. In addition, DPSC dECM or DPSC sheets increased the migration

and neurogenic differentiation of NSCs, reduced the formation of glial scars, regulated the immune microenvironment after SCI in vivo and facilitated the migration and neurogenesis of NSCs in vitro. Thus, DPSC dECM and DPSC sheets have great potential for clinical application in the treatment of SCI.

It has been reported that cell-derived ECM can influence cell migration, direct cell differentiation, and induce host tissue repair and bone tissue, cartilage tissue and nerve tissue regeneration.[10,11,24,25] These effects are related to the 3D architecture and composition of the ECM. It is important to find the optimal method for the preparation of DPSC dECM that can remove as many cell components as possible, minimize the loss of major matrix components and retain good bioactivity to promote cell growth or tissue reconstruction. To date, the most commonly used methods for decellularization include physical or mechanical methods, chemical methods, treatment with biological agents and their combination.[9] At present, there is no unified standard method for decellularization, and the proper method needs to be chosen according to the source, ECM thickness, application field, etc. Physical methods usually cause damage to the ECM structure and are more suitable for the decellularization of large tissues or organs.[26,27] Chemical methods alone may lead to a substantial loss of bioactive proteins, while enzyme digestion alone fails to completely remove cell debris.[26,28] Mild detergents, such as Triton X-100, are commonly used for the decellularization of tissues such as cell layers.[9,29] Studies have shown that Triton X-100 can effectively remove cell residues, causing minimal disruption of GAG, growth factors, collagen, and other components in the ECM, unlike the ionic surfactant sodium dodecyl sulfate (SDS).[30,31] However, Triton X-100 removes only a small amount of residual DNA,[32] so it is necessary to use it in combination with DNase (Deoxyribonuclease enzyme). Farag et al.[33] reported that treatment with the combination of Triton X-100 and DNase was more for preserving ECM integrity and retaining growth factors in periodontal ligament cell sheets than the freeze–thaw cycling method and treatment with SDS. Therefore, we used Triton X-100 combined with DNase to decellularize DPSC sheets based on the methods described above.[11,33,34] To date, there has been no research on specific methods for the decellularization of DPSC sheets. Hence, we used two different concentrations of Triton X-100 and three different treatment durations to select the best conditions for the decellularization of DPSC sheets based on existing studies.

The success of decellularization was evaluated from two aspects: the removal of cell components and maintenance of the integrity and bioactivity of the ECM. The removal of cell components was evaluated by H&E staining, quantification of DNA content and DAPI staining, while the integrity of the ECM was evaluated by SEM and collagen I staining. H&E staining and DAPI staining revealed that there were no cell components in any of the treatment groups except for the 0.5% Triton X-100 5 min group, indicating that this condition had low decellularization efficiency. In the present study, we successfully removed more than 98% of DNA through treatment with 1% Triton X-100 for 5 min; these findings were comparable to the findings of Sadr et al.,[35] who reported that removal of 94% of DNA during decellularization had no adverse effects on the effect of ECM implantation in vivo. A study by Syedain et al.[23] reported that removing more than 99% of the DNA may damage ECM integrity, indicating that the bioactivity of the ECM in the 1% Triton X-100 10 min group and 1% Triton X-100 30 min group may have been seriously impaired. Furthermore, we performed fluorescence staining for collagen I, which is a predominant protein in the ECM, to investigate whether the integrity of the ECM was maintained. We were able to demonstrate its presence, and the mean fluorescence intensity of collagen I in the 1% Triton X-100 5 min group was comparable to that in the DPSC sheets before decellularization. SEM analysis of DPSC dECM in the 1% Triton X-100 5 min group revealed the presence of a fine network of ECM fibers with a morphology and structural integrity similar to that observed in the DPSC sheet; these results were comparable to what was observed for cell-derived dECM prepared by incubation with Triton X-100 solution for 5 min in other studies.[34,36] When the Triton X-100 treatment time was extended to 10 min or 30 min, the fiber networks became more irregular and were severely disrupted. Collectively, these results indicated that 1% Triton X-100 solution for 5 min was the best condition for decellularizing DPSC sheets in this study; this treatment not only effectively removed cellular components but also maintained the integrity of the ECM.

After SCI, the hostile environment of the lesion inhibits axonal regeneration. Therefore, engineered biomaterials may play a vital role in providing a suitable microenvironment for neural regeneration. In this study, we transplanted DPSC dECM and DPSC sheets into the lesion site of spinal cord hemisection model rats to promote axonal regeneration and functional recovery. Both DPSC dECM and DPSC sheets are natural scaffold-free materials that are biocompatible and degradable in vivo.[9] In this study, we found that DPSC dECM and DPSC sheets were degraded in vivo, which was similar to the findings of studies involving transplantation of ECM-based materials for tissue regeneration.[24,25,37] DPSC dECM and DPSC sheets promoted NSC migration to the site of injury and regulated the immune microenvironment, subsequently promoting nerve regeneration and reducing the formation of glial scars. It was reported that bioactive factors produced by ECM degradation can recruit endogenous progenitor/stem cells to the lesion site and regulate the infiltration and polarization of macrophages, subsequently facilitating the self-healing of lesions.[38–41] However, the ECM degradation rate and underlying mechanisms should be further investigated.

It has been reported that dECM can provide a 3D architecture and bioactive components to support neuronal differentiation and axonal regeneration. Previous studies have shown that grafted spinal cord tissue-derived dECM or brain tissue-derived dECM could increase the number of NF-positive nerve fibers at the injury site.[7,8] In the present study, we also found that grafted DPSC dECM could reduce the size of the lesion cavity and trigger NF-positive neurite sprouting to bridge the lesion gap. Considering its ease of preparation and low risk of disease transmission, our cell-derived dECM material may be more suitable for clinical applications than other ECM materials.

The recruitment of NSCs to the site of injury and their functionalization are essential for regenerative repair. In the present study, we found that DPSC dECM promoted the migration of NSCs and increased the expression of NF, indicating that dECM might provide a suitable microenvironment for the recruitment and functionalization of NSCs through exosomes or other forms of delivery.[42] Studies have shown that with the aging of cells, exosomes change to a senescence-associated secretory phenotype,

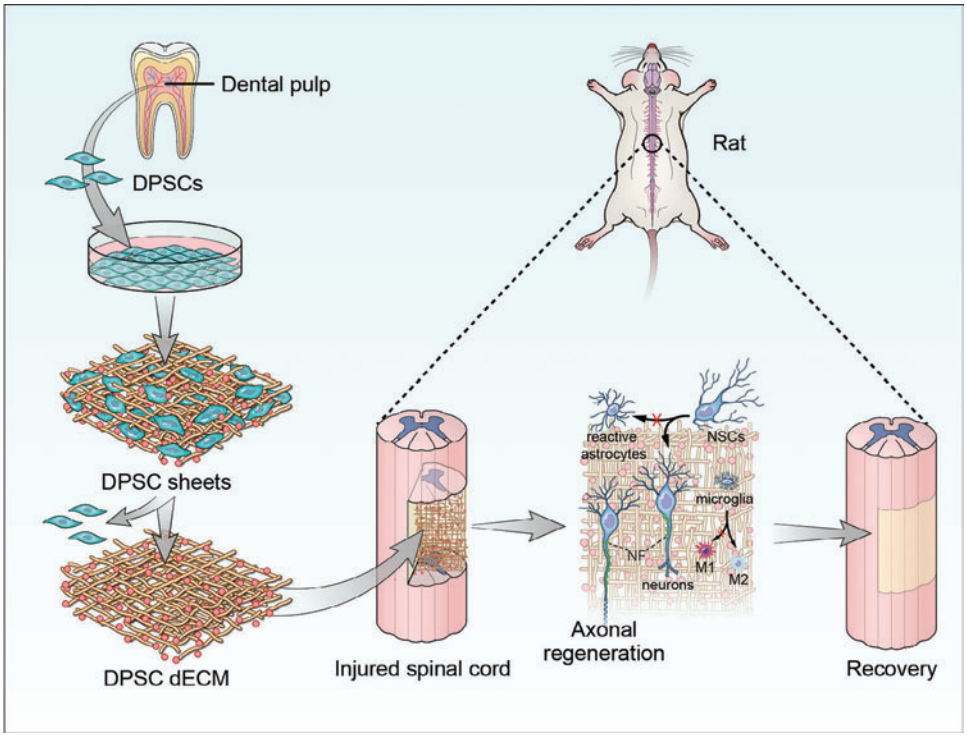

Figure 9. Preparation of decellularized extracellular matrix from dental pulp stem cell sheets (DPSC dECM) and its application in injured spinal cord repair. We optimize the preparation of DPSC dECM and transplant it into a rat SCI model and demonstrate a potential strategy of DPSC dECM promoted migration and neurogenic differentiation of neural stem cells, reduced the formation of glial scars, regulated the immune microenvironment to execute the axonal regeneration, functional recovery.

which may affect the biological function and therapeutic efficacy of dECM.[43] However, cultivation of cells without passaging, such as in the case of cell sheets, helps telomerase play a compensatory role; thus, dECM obtained through this method has a stronger curative effect.[44] NF, which is a specific structural protein that is expressed in mature neurons, plays an essential role in neuron differentiation and axon regeneration. In our study, the number of NF-positive cells at the SCI site was increased in the DPSC dECM group, and the expression of NF in NSCs was upregulated after coculture with DPSC dECM in vitro. These phenomena could be related to the bioactive molecules originating from dECM. Proteomic analysis demonstrated that spinal cord tissue-derived dECM is rich in LAMA1 and LAMB1, which are related to the adhesion of NSCs, and rich in TNC and FGF2, which can promote the neural differentiation of NSCs.[7] Proteomic analysis of dental pulp tissue-derived dECM revealed that it contains 26 proteins related to cell migration, including ACTN4 and FLNA, and more than 30 proteins related to neurogenesis, such as NES, TUBB3, NEFH, and MAP1B.[45] However, dental pulp tissue contains a variety of cells, and the proteins expressed in dental pulp tissue-derived dECM may be different from that of DPSC dECM. Therefore, proteomic analysis of DPSC dECM should be performed.

Interestingly, we found that the DPSC sheets exerted similar effects in promoting axonal regeneration, functional recovery and NSC migration and differentiation as DPSC dECM. Unlike DPSC sheets, the presence of DPSCs in the sheet could not further promote the migration and neural differentiation of NSCs; therefore, it was hypothesized that ECM components might play a major role in the migration and differentiation of NSCs.

4. Conclusion

In summary, we successfully optimized the protocol for the generation of DPSC dECM and showed that incubating DPSC sheets with a 1% Triton X-100 solution for 5 min was the optimal decellularization procedure. Furthermore, the results of the present study demonstrated that DPSC dECM promoted neural regeneration and functional recovery after SCI by facilitating NSC migration and differentiation, inhibiting glial scar formation, and regulating the immune microenvironment, suggesting that DPSC dECM is a potential therapeutic agent for the treatment of SCI (**Figure 9**).

5. Experimental Section

DPSC Isolation, Culture, and Identification: DPSCs were harvested from the molars or premolars of five donors (aged 20–25 years) who requested tooth extraction for orthodontic treatment at the Department of Stomatology, Nanfang Hospital, Southern Medical University. This study was approved by the Ethics Committee of Nanfang Hospital, Southern Medical University (NFEC-2023-080), and informed consent was obtained from the donors. DPSCs were isolated from dental pulp tissues and cultured as previously described.[46] The cells were seeded in 100-mm dishes at a density of 1×10^5 cells per dish and cultured in complete medium composed of alpha minimum essential medium (αMEM; Gibco/BRL,

Cheshire, UK), 10% fetal bovine serum (FBS (Fetal bovine serum); Biowest, France) and 1% penicillin–streptomycin-amphotericin B suspension (PSA; WAKO Pure Chemical Industries, Osaka, Japan). A limited dilution technique was used to obtain colonies of single-cell origin.[47] The cells were passaged when they reached 80% confluence. DPSCs between passages 3 and 5 were used in all experiments. The cells were incubated at 37°C in 5% CO_2. The culture medium was replaced every 3 days.

The cells were characterized by analyzing stem cell surface marker expression by flow cytometry (Becton Dickinson, Tokyo, Japan). For intracellular antigen staining, DPSCs were suspended in phosphate-buffered saline (PBS) supplemented with 2% FBS and incubated with antibodies on ice for 30 min. The following antibodies were used: anti-phycoerythrin (PE) and anti-fluorescein isothiocyanate (FITC) (BD Pharmingen, Franklin Lakes, NJ). Isotype-control antibodies were used as controls. All procedures were carried out in the dark at 4°C. Marker expression was analyzed by flow cytometry.

Osteogenic, Adipogenic, and Neurogenic Differentiation: Osteogenic, adipogenic, and neurogenic differentiation were induced to determine the potential of DPSCs to differentiate into multiple cell types. Second generation DPSCs were digested with 0.25% trypsin, the concentration was adjusted, and the cells were subsequently inoculated into 6-well plates at a density of 1×10^5 cells/well. When the cells had reached 80% confluence, the complete medium was replaced with osteogenic (containing 10% FBS, 50 mg mL^{-1} ascorbic acid, 100 nmol l^{-1} dexamethasone, and 10 mmol l^{-1} β-glycerophosphate), adipogenic (containing 10% FBS, 0.5 mM isobutylmethylxanthine (IBMX), 10^{-6} M dexamethasone, 10 µg mL^{-1} insulin, and 200 µM indomethacin), or neurogenic (20 ng mL^{-1} EGF (Beyotime, China) and 20 ng mL^{-1} bFGF (Beyotime, China)) induction medium. DPSCs in the undifferentiated group were cultured in α-MEM supplemented with 10% FBS but not with other reagents. The cells were incubated at 37°C in 5% CO_2. The culture medium was replaced every 3 days. After 14 days of osteogenic or adipogenic differentiation, mineralized nodules were stained with 1% Alizarin Red S (Sigma–Aldrich, USA), and lipid droplets were visualized via Oil Red O staining (Sigma–Aldrich, USA) following a standard protocol.

Optimized Preparation of dECM Derived from DPSC Sheets: To form DPSC sheets, cells were seeded in 6-well plates at a concentration of 2×10^5 cells $well^{-1}$ in complete medium. When the DPSCs had reached 80–90% confluence, the medium was removed and replaced with high-glucose DMEM supplemented with 10% FBS, 50 µg mL^{-1} ascorbic acid and 1% penicillin–streptomycin-amphotericin B suspension. The cells were continuously cultured for 14 days at 37°C in 5% CO_2, and the medium was changed every 2 days. At the end of the 14-day culture period, the borders of the DPSC sheets were gently detached from the base of the well, and the sheets were easily lifted with a cell scraper and harvested for further experiments.

dECM derived from decellularized DPSC sheets was prepared by incubating DPSC sheets with Triton X-100 supplemented with 20 mM NH_4OH. Two different concentrations of Triton X-100, namely, 0.5% and 1%, and three different processing times, namely, 5, 10, and 30 min, were used to determine the optimum conditions for generating DPSC dECM. After 14 days of culture, the DPSC sheets were lifted with a cell scraper, washed three times in PBS, and then incubated in 0.5% or 1% Triton X-100 at 37°C for 5, 10, or 30 min. Then, the DPSC sheets from the different groups were washed three times in PBS and treated with 100 U mL^{-1} deoxyribonuclease enzyme (DNase) (Solarbio, China) at 37°C for 1 h to remove any possible residual cellular components. After the decellularization process, part of the harvested DPSC dECM was processed for histological analysis, biochemical assays, and scanning electronic microscopy (SEM) (Hitachi, Japan).

Quantification of DNA Content: The DNA contents of DPSC sheets and DPSC dECM from the different groups were measured to determine the degree of cell removal by using the FitAmp™ General DNA Quantification Kit (Epigentek, USA) after the matrix was digested with proteinase K (Beyotime, China). Then, a fluorescence microplate reader (Molecular Devices, USA) was used to quantify the DNA content by measuring the fluorescence at Ex 480–500 and Em 520–550 nm. The tests were conducted three times.

Cytotoxicity Assay: The cytotoxicity of dECM was investigated by a CCK8 assay (Fdbio Science, China). DPSC sheets and DPSC dECM from six different groups were placed in 15-mL sterilized centrifuge tubes, and 5 mL of high-glucose DMEM supplemented with 10% FBS was added to each tube. Then, the tubes were incubated with continuous physical agitation (150 rpm on an orbital shaker) at 37°C in 5% CO_2 for 24 h. The supernatants (hereafter referred to as the ECM extracts) were collected for subsequent cytotoxic assays. C17.2 neural stem cells (NSCs) were used for the CCK8 assay. C17.2 NSCs were obtained from the Department of Neurology of the Third Affiliated Hospital of Southern Medical University of Guangzhou. First, NSCs were seeded in 96-well plates at a concentration of 3×10^3 cells $well^{-1}$ and cultured in complete medium composed of high-glucose DMEM supplemented with 10% FBS. After the cells had adhered, the culture medium was changed to fresh medium (blank control medium) containing ECM extracts from DPSC sheets or DPSC dECM from the different groups. The NSCs were cultured for 6 days, and the medium of each group was changed every day. On each day of the assay, 10 µL of CCK8 solution was added to each well, and the cells were further incubated at 37°C for 1 h in the dark. After incubation, a microplate reader (Molecular Devices, USA) was used to measure the optical density at 450 nm. All the ECM extracts were prepared as described above, and six replicates of each sample were used for the CCK8 assay.

Animal Surgery: The animal protocols were reviewed and approved by the Institutional Animal Care and Use Committee of Nanfang Hospital of Southern Medical University (NFYY-2021-0619), Guangzhou, China. All animals were housed in a temperature- and humidity-controlled SFP animal facility on a 12-h light/dark cycle. Forty-eight adult male Sprague–Dawley rats (6-8 weeks old, weighing 200 g-300 g) were purchased from the Animal Center of Southern Medical University. Food and water were available ad libitum. The rats were randomly divided into three groups for in vivo study: the control group, DPSC sheet group, and DPSC dECM group ($n = 8$ for day 7, $n = 8$ for day 28 in each group). Locomotor function was assessed weekly before and after surgery with the BBB locomotor rating scale, and footprint analysis was performed on day 28. Histological examinations were performed on day 7 and day 28.

After anesthesia, a 3 cm midline incision was made in the skin on the backs of the rats to expose the T9-T11 vertebrae. The muscles were cut in layers along the midline, and laminectomy was performed at the T9-10 level to expose the T10 spinal cord segment. Under a microscope, hemisection of the right T10 spinal cord was then performed using iris microscissors and ophthalmic microforceps, creating a lateral hemisection lesion with a width of 2 mm. After sufficient hemostasis with a gelatin sponge, the muscle and skin layers were closed using 4–0 silk sutures. To prevent infection, the rats were subcutaneously injected with ampicillin (100 mg kg^{-1}) once a day for 3 days after surgery. Manual bladder expression was performed twice a day until the rats regained bladder control, which occurred ≈3 to 5 days after the initial injury.

Histological Analysis: Spinal cord tissues and visceral tissues (heart, liver, spleen, lung, and kidney) were fixed with 4% paraformaldehyde for 24 h and transferred to 75% ethanol. The tissues were embedded in paraffin, and 5-µm sections were prepared. H&E staining (Leagene Biotechnology, China) was performed according to the manufacturer's instructions. Regions of interest (ROIs) were observed via microscopy (BX63; Olympus, USA).

Immunofluorescence Analysis: Spinal cord tissue sections were prepared as previously described. The sections were deparaffinized with xylene and rehydrated in a graded series of alcohol solutions, followed by antigen retrieval. The sections were incubated overnight at 4°C with antibodies against glial fibrillary acidic protein (GFAP) (1:200; Proteintech, Wuhan, China), nestin (1:200; ABclonal, Wuhan, China), neurofilament (NF) (1:200; Proteintech, Wuhan, China), chondroitin sulfate (CS56) (1:200; Sigma–Aldrich, USA), CD68 (1:200; Servicebio, Wuhan, China) and CD206 (1:500; Proteintech, Wuhan, China). The sections were washed and incubated with secondary antibodies for 1 h at room temperature. The cell nuclei were stained with 4',6-diamidino-2-phenylindole (DAPI). The sections were then mounted with glycerol jelly mounting medium. Images of selected fields were captured via microscopy (BX63; Olympus, USA).

Table 1. The primer sequences.

Target genes	Sequence
nestin	Forward: CTGCTACCCTTGAGACACCTG
	Reverse: GGGCTCTGATCTCTGCATCTAC
β3-TUBULIN	Forward: GGCCTCTTCTCACAAGTACG
	Reverse: CCACTCTGACCAAAGATGAAA
GAP43	Forward: GGCCGCAACCAAAATTCAGG
	Reverse: CGGCAGTAGTGGTGCCTTC
NF	Forward: GTGAAGAGTGTCGGATTGGCT
	Reverse: ACACAGAGGGAATTTTGGGGA
GAPDH	Forward: CTGGGCTACACTGAGCACC
	Reverse: AAGTGGTCGTTGAGGGCAATG

Locomotor Function Recovery Assessment: The BBB scale was used to measure the recovery of left hind limb function in SCI model rats after the transplantation of DPSC dECM.[48] Briefly, individual rats from the three groups were placed in an open field and observed for 4 min by two observers who were blinded to the treatments. The test was conducted once a week after transplantation for up to 4 weeks. Footprint analysis was performed on day 28 after transplantation. After the hind limbs of the rats in the three groups were painted with red ink, the rats were placed on paper (size 594 mm × 841 mm), and each individual rat was allowed to move freely for 2 min. A 30 cm straight line of footsteps was chosen for analysis. The experiments were performed in triplicate.

Transwell Chemotaxis Assay: A 12-well transwell plate (Corning, USA) was used to evaluate the effect of DPSC dECM on NSC migration. Three groups were used in this assay: 1) the control group, which was treated with standard high-glucose DMEM; 2) the standard high-glucose DMEM plus DPSC sheet group; and 3) the standard high-glucose DMEM plus DPSC dECM group. A piece of DPSC sheet or DPSC dECM from one well of a six-well plate was placed in each transwell insert. Then, 200 µL of NSCs were seeded in the upper chamber at a density of 1×10^5 cells/well for each group. Standard high-glucose DMEM supplemented with 1% FBS without DPSC sheets or DPSC dECM was added to the lower chamber as a control, while 700 µL of standard high-glucose DMEM supplemented with 1% FBS and containing DPSC sheets or DPSC dECM was added to the lower chamber as a stimulus. After 12 h of incubation at 37°C in 5% CO_2, the medium in the upper chamber was carefully removed, the nonmigrating cells in the upper chamber were carefully scraped away with cotton swabs, and the upper chamber was washed with PBS. The upper chamber was then carefully transferred to the lower chamber; the medium was replaced with 700 µL of 10% formaldehyde to fix the migrated cells that attached to the lower side of the upper chamber, and the cells were incubated for 30 min at room temperature. Next, the cells were incubated with 0.1% crystal violet (Leagene, Chain) for 15 min to stain the migrated cells. A total of three fields of each well were analyzed at 200× magnification to determine the mean number of migrated cells with ImageJ software.

qRT–PCR: To assess the neurogenic differentiation of DPSCs, total RNA was isolated from the two groups of hDPSCs by an EZ-press RNA Purification Kit (EZBioscience, USA). One microgram of RNA per sample was reverse transcribed into cDNA using a Color Reverse Transcription Kit (EZBioscience, USA). qRT-PCR was performed in a 10 µL reaction system using 2 × Color SYBR Green qPCR Master Mix (EZBioscience, USA) on a Roche LightCycler 480 sequence detection system. Glyceraldehyde-3-phosphate dehydrogenase (GAPDH/gapdh) was used as an internal control. The sequences of the gene-specific primers used are listed in **Table 1**. Relative gene expression is presented as the fold change calculated with the $2^{-\Delta\Delta Ct}$ method, and the experiments were performed in triplicate.

Western Blotting: To assess the effect of DPSC dECM on the neural differentiation of NSCs, NSCs. and DPSC dECM were cocultured in vitro, and the response of NSCs to neurogenic induction conditions was investigated. A total of three groups were used in the study: 1) 1×10^4 NSCs/well cultured in neurogenic medium; 2) 1×10^4 NSCs/well cultured in neurogenic medium and a piece of DPSC sheet (from one well of a six-well plate) placed in a transwell chamber; and 3) 1×10^4 NSCs/well cultured in neurogenic medium and a piece of DPSC dECM (from one well of a six-well plate) placed in a transwell chamber. The neurogenic medium was composed of DMEM-F12 supplemented with 1% N2 supplement (Stem Cell, USA), 10 ng mL^{-1} BDNF (Brain-derived neurotrophic factor) (Novoprotein, China), and 10 ng mL^{-1} NGF (Novoprotein, China). The NSCs in the previously mentioned groups were continuously cultured for 14 days in a 5% CO_2 cell culture incubator at 37°C, and the medium was changed every 2 days. After being cocultured for 2 weeks, C17.2 NSCs were lysed in RIPA lysis buffer supplemented with protease inhibitors on ice for 30 min to collect total protein. The proteins were separated by 10% SDS–PAGE and transferred to PVDF membranes. The membranes were blocked with 5% BSA and then incubated with primary antibodies (NF, 1:500, Proteintech; β3-TUBULIN, 1:500, Cell Signaling Technology) followed by secondary antibodies. Finally, images were acquired via an enhanced chemiluminescence system (BLT GelView 6000 Pro scanner, BLT, Guangzhou, China), and the densities of the immunoreactive bands were quantified via ImageJ software.

ELISA: At 28 days postinjury (dpi), blood was collected from the hearts of the rats. After coagulation at room temperature for 30 min, the blood was centrifuged at 15 000 rpm for 15 min, after which the supernatant was collected. IFN-γ and IL-10 levels were measured using ELISA kits and a microplate reader (ELGBIO, Guangzhou, China; Infinite F50 Plus, TECAN, Switzerland) according to the manufacturer's instructions.

Statistical Analysis: The data are expressed as the mean ± standard error (SE), and the assays were repeated at least three times. Statistical analysis was performed by t test or one-way ANOVA using GraphPad Prism 9.0.0 for Windows (GraphPad Prism, USA). Statistical significance was defined as $^*P < 0.05$, $^{**}P < 0.01$, $^{***}P < 0.001$, and $^{****}P < 0.0001$.

Supporting Information

Supporting Information is available from the Wiley Online Library or from the author.

Acknowledgements

This work was supported by the National Natural Science Foundation of China [82270982 and 82101024], the Guangdong Basic and Applied Basic Research Foundation (2024A1515010840), the Guangzhou Science and Technology Plan Project [2023A04J0426, 2024A04J5105, and 2024B03J0667] and the grant from Guangdong Provincial Key Laboratory of Oral Diseases [KF2022120103].

Conflict of Interest

The authors declare no conflict of interest.

Author Contributions

W.Q., B.Z., Y.L., and Y.C. contributed equally and co-first authors to this work. W.Q. and F.F. contributed to the conception and design of the research and the critical revision of the manuscript. B.Z., Y.L., and Y.C. contributed to performing the experimental work and writing the manuscript. Z.C., K.W., and H.W. contributed to drawing the figures and tables and analyzing the data. B.W. and J.G. contributed to the critical revision of the manuscript for important intellectual content. All authors critically reviewed and approved the final version of the manuscript.

Data Availability Statement

The data that support the findings of this study are available from the corresponding author upon reasonable request.

Keywords

decellularized extracellular matrix, dental pulp stem cells, neural regeneration, neural stem cells, spinal cord injury

Received: June 24, 2024
Revised: August 7, 2024
Published online:

[1] J. M. Schwab, K. Brechtel, C. A. Mueller, V. Failli, H. P. Kaps, S. K. Tuli, H. J. Schluesener, *Prog Neurobiol* **2006**, *78*, 91.
[2] L. Wang, S. Gu, J. Gan, Y. Tian, F. Zhang, H. Zhao, D. Lei, *Front Cell Neurosci* **2021**, *15*, 773375.
[3] I. Eli, D. P. Lerner, Z. Ghogawala, *Neurol Clin.* **2021**, *39*, 471.
[4] T. Tykocki, Ł. Poniatowski, M. Czyż, M. Koziara, G. Wynne-Jones, *World Neurosurg* **2017**, *105*, 145.
[5] *J. Spinal Cord Med* **2008**, *31*, 403.
[6] Z. Wang, C. Chai, R. Wang, Y. Feng, L. Huang, Y. Zhang, X. Xiao, S. Yang, Y. Zhang, X. Zhang, *Clin. Transl. Med.* **2021**, *11*, e650.
[7] Y. Xu, J. Zhou, C. Liu, S. Zhang, F. Gao, W. Guo, X. Sun, C. Zhang, H. Li, Z. Rao, S. Qiu, Q. Zhu, X. Liu, X. Guo, Z. Shao, Y. Bai, X. Zhang, D. Quan, *Biomaterials* **2021**, *268*, 120596.
[8] J. Y. Hong, Y. Seo, G. Davaa, H. W. Kim, S. H. Kim, J. K. Hyun, *Acta Biomater.* **2020**, *101*, 357.
[9] W. Zhang, Y. Zhu, J. Li, Q. Guo, J. Peng, S. Liu, J. Yang, Y. Wang, *Tissue Eng Part B Rev.* **2016**, *22*, 193.
[10] C. Xue, H. Ren, H. Zhu, X. Gu, Q. Guo, Y. Zhou, J. Huang, S. Wang, G. Zha, J. Gu, Y. Yang, Y. Gu, X. Gu, *J. Mater. Chem. B* **2017**, *5*, 1246.
[11] B. Xiao, F. Rao, Z. Y. Guo, X. Sun, Y. G. Wang, S. Y. Liu, A. Y. Wang, Q. Y. Guo, H. Y. Meng, Q. Zhao, J. Peng, Y. Wang, S. B. Lu, *Neural Regen Res.* **2016**, *11*, 735.
[12] G. M. Harris, N. N. Madigan, K. Z. Lancaster, L. W. Enquist, A. J. Windebank, J. Schwartz, J. E. Schwarzbauer, *Matrix Biol.* **2017**, *60–61*, 176.
[13] C. C. Chang, K. C. Chang, S. J. Tsai, H. H. Chang, C. P. Lin, *J. Formos. Med. Assoc.* **2014**, *113*, 956.
[14] X. Zhang, T. Ning, H. Wang, S. Xu, H. Yu, X. Luo, C. Hao, B. Wu, D. Ma, *J. Proteomics* **2019**, *202*, 103364.
[15] S. Gronthos, J. Brahim, W. Li, L. W. Fisher, N. Cherman, A. Boyde, P. DenBesten, P. G. Robey, S. Shi, *J. Dent. Res.* **2002**, *81*, 531.
[16] E. Karaöz, P. C. Demircan, O. Sağlam, A. Aksoy, F. Kaymaz, G. Duruksu, *Histochem. Cell Biol* **2011**, *136*, 455.
[17] Y. Fujii, Y. Kawase-Koga, H. Hojo, F. Yano, M. Sato, U. I. Chung, S. Ohba, D. Chikazu, *Stem Cell Res. Ther.* **2018**, *9*, 24.
[18] K. Sakai, A. Yamamoto, K. Matsubara, S. Nakamura, M. Naruse, M. Yamagata, K. Sakamoto, R. Tauchi, N. Wakao, S. Imagama, H. Hibi, K. Kadomatsu, N. Ishiguro, M. Ueda, *J. Clin. Invest.* **2012**, *122*, 80.
[19] Y. Chen, H. Huang, G. Li, J. Yu, F. Fang, W. Qiu, *Stem Cell Res. Ther.* **2022**, *13*, 38.
[20] S. Guo, I. Redenski, S. Landau, A. Szklanny, U. Merdler, S. Levenberg, *Adv. Healthcare Mater.* **2020**, *9*, e2000974.
[21] Y. Ying, Z. Huang, Y. Tu, Q. Wu, Z. Li, Y. Zhang, H. Yu, A. Zeng, H. Huang, J. Ye, W. Ying, M. Chen, Z. Feng, Z. Xiang, Q. Ye, S. Zhu, Z. Wang, *Bioact. Mater.* **2023**, *22*, 274.
[22] S. Zhu, Y. Ying, Y. He, X. Zhong, J. Ye, Z. Huang, M. Chen, Q. Wu, Y. Zhang, Z. Xiang, Y. Tu, W. Ying, J. Xiao, X. Li, Q. Ye, Z. Wang, *Bioact Mater* **2021**, *6*, 2452.
[23] Z. H. Syedain, A. R. Bradee, S. Kren, D. A. Taylor, R. T. Tranquillo, *Tissue Eng Part A* **2013**, *19*, 759.
[24] Z. Wang, L. Han, T. Sun, J. Ma, S. Sun, L. Ma, B. Wu, *Acta Biomater.* **2020**, *118*, 54.
[25] Z. Wang, Z. Li, Z. Li, B. Wu, Y. Liu, W. Wu, *Acta Biomater.* **2018**, *81*, 129.
[26] M. J. Buckenmeyer, T. J. Meder, T. A. Prest, B. N. Brown, *Methods* **2020**, *171*, 41.
[27] S. Funamoto, K. Nam, T. Kimura, A. Murakoshi, Y. Hashimoto, K. Niwaya, S. Kitamura, T. Fujisato, A. Kishida, *Biomaterials* **2010**, *31*, 3590.
[28] Q. Xing, K. Yates, M. Tahtinen, E. Shearier, Z. Qian, F. Zhao, *Tissue Eng Part C Methods* **2015**, *21*, 77.
[29] S. R. Meyer, B. Chiu, T. A. Churchill, L. Zhu, J. R. Lakey, D. B. Ross, *J. Biomed. Mater. Res., Part A* **2006**, *79*, 254.
[30] H. C. Ott, B. Clippinger, C. Conrad, C. Schuetz, I. Pomerantseva, L. Ikonomou, D. Kotton, J. P. Vacanti, *Nat. Med.* **2010**, *16*, 927.
[31] J. E. Reing, B. N. Brown, K. A. Daly, J. M. Freund, T. W. Gilbert, S. X. Hsiong, A. Huber, K. E. Kullas, S. Tottey, M. T. Wolf, S. F. Badylak, *Biomaterials* **2010**, *31*, 8626.
[32] D. C. Sullivan, S. H. Mirmalek-Sani, D. B. Deegan, P. M. Baptista, T. Aboushwareb, A. Atala, J. J. Yoo, *Biomaterials* **2012**, *33*, 7756.
[33] A. Farag, S. M. Hashimi, C. Vaquette, F. Z. Volpato, D. W. Hutmacher, S. Ivanovski, *Arch. Oral Biol.* **2018**, *88*, 67.
[34] X. Xiong, X. Yang, H. Dai, G. Feng, Y. Zhang, J. Zhou, W. Zhou, *Stem Cell Res. Ther.* **2019**, *10*, 396.
[35] N. Sadr, B. E. Pippenger, A. Scherberich, D. Wendt, S. Mantero, I. Martin, A. Papadimitropoulos, *Biomaterials* **2012**, *33*, 5085.
[36] X. D. Chen, V. Dusevich, J. Q. Feng, S. C. Manolagas, R. L. Jilka, *J. Bone Miner Res* **2007**, *22*, 1943.
[37] A. Okuda, N. Horii-Hayashi, T. Sasagawa, T. Shimizu, H. Shigematsu, E. Iwata, Y. Morimoto, K. Masuda, M. Koizumi, M. Akahane, M. Nishi, Y. Tanaka, *J. Neurosurg Spine* **2017**, *26*, 388.
[38] E. Vorotnikova, D. McIntosh, A. Dewilde, J. Zhang, J. E. Reing, L. Zhang, K. Cordero, K. Bedelbaeva, D. Gourevitch, E. Heber-Katz, S. F. Badylak, S. J. Braunhut, *Matrix Biol.* **2010**, *29*, 690.
[39] V. Agrawal, S. A. Johnson, J. Reing, L. Zhang, S. Tottey, G. Wang, K. K. Hirschi, S. Braunhut, L. J. Gudas, S. F. Badylak, *Proc. Natl. Acad. Sci. USA* **2010**, *107*, 3351.
[40] W. Cao, S. Peng, Y. Yao, J. Xie, S. Li, C. Tu, C. Gao, *Acta Biomater.* **2022**, *152*, 60.
[41] S. Hauck, P. Zager, N. Halfter, E. Wandel, M. Torregrossa, A. Kakpenova, S. Rother, M. Ordieres, S. Räthel, A. Berg, S. Möller, M. Schnabelrauch, J. C. Simon, V. Hintze, S. Franz, *Bioact Mater* **2021**, *6*, 4342.
[42] S. Li, L. Luo, Y. He, R. Li, Y. Xiang, Z. Xing, Y. Li, A. A. Albashari, X. Liao, K. Zhang, L. Gao, Q. Ye, *Cell Proliferation* **2021**, *54*, e13093.
[43] S. Jing, H. Zhou, C. Zou, D. P. C. Chen, Q. Ye, Y. Ai, Y. He, *Nano TransMed* **2022**, *1*, e9130007.
[44] N. Pilbauerova, T. Soukup, K. T. Suchankova, J. Schmidt, J. Suchanek, *Biomolecules* **2021**, *11*, 464.
[45] J. Li, Z. Rao, Y. Zhao, Y. Xu, L. Chen, Z. Shen, Y. Bai, Z. Lin, Q. Huang, *J Endod.* **2020**, *46*, 1438.
[46] L. Cui, S. Xu, D. Ma, J. Gao, Y. Liu, J. Yue, B. Wu, *J Endod.* **2014**, *40*, 235.
[47] Y. Ge, J. Li, Y. Hao, Y. Hu, D. Chen, B. Wu, F. Fang, *J Periodontal Res.* **2018**, *53*, 832.
[48] D. M. Basso, M. S. Beattie, J. C. Bresnahan, *J Neurotrauma.* **1995**, *12*, 1.